Atmospheric correction for NO$_2$ absorption in retrieving water-leaving reflectances from the SeaWiFS and MODIS measurements

Ziauddin Ahmad,[1,2,*] Charles R. McClain,[1] Jay R. Herman,[1] Bryan A. Franz,[1,3]
Ewa J. Kwiatkowska,[1,3] Wayne D. Robinson,[1,3] Eric J. Bucsela,[1,4] and Maria Tzortziou[1,5]

[1]NASA Goddard Space Flight Center, Greenbelt, Maryland 20771, USA
[2]Science and Data Systems, Inc., 16509 Copperstrip Lane, Silver Spring, Maryland 20906, USA
[3]Science Applications International Corporation, 10260 Campus Point Drive, San Diego, California 92121, USA
[4]University of Maryland, Baltimore County, Maryland 21250, USA
[5]University of Maryland, College Park, Maryland 20742, USA

*Corresponding author: ahmad@seawifs.gsfc.nasa.gov

The absorption by atmospheric nitrogen dioxide (NO$_2$) gas in the visible has been traditionally neglected in the retrieval of oceanic parameters from satellite measurements. Recent measurements of NO$_2$ from spaceborne sensors show that over the Eastern United States the NO$_2$ column amount often exceeds 1 Dobson Unit ($\sim$2.69 $\times$ 10^{16} molecules/cm^2). Our radiative transfer sensitivity calculations show that under high NO$_2$ conditions ($\sim$1 $\times$ 10^{16} molecules/cm^2) the error in top-of-atmosphere (TOA) reflectance in the blue channels of the sea-viewing wide field-of-view sensor (SeaWiFS) and moderate-resolution imaging spectroradiometer (MODIS) sensors is approximately 1%. This translates into approximately 10% error in water-leaving radiance for clear waters and to higher values ($>$20%) in the coastal areas. We have developed an atmospheric-correction algorithm that allows an accurate retrieval of normalized water-leaving radiances (nLws) in the presence of NO$_2$ in the atmosphere. The application of the algorithm to 52 MODIS scenes over the Chesapeake Bay area show a decrease in the frequency of negative nLw estimates in the 412 nm band and an increase in the value of nLws in the same band. For the particular scene reported in this paper, the mean value of nLws in the 412 nm band increased by 17%, which is significant, because for the MODIS sensor the error in nLws attributable to the digitization error in the observed TOA reflectance over case 2 waters is $\sim$2.5%.   © 2007 Optical Society of America

OCIS codes: 010.1310, 010.4450, 290.1310, 290.4210, 290.5890.

1. Introduction

Atmospheric nitrogen dioxide (NO$_2$) is an important trace gas that plays a major role in the destruction of ozone in the middle stratosphere and production of ozone in the lower troposphere [1]. In the stratosphere, NO$_2$ is mainly produced by photodissociation of the NO$_2$ reservoir species. In the lower troposphere (1–3 km), the primary sources of NO$_2$ production are industries, automobiles, and biomass burning. These sources, together with emission from the soil, account for most of the NO$_2$ in the atmosphere.

NO$_2$ has a broad absorption spectrum that extends from UV ($\sim$270 nm) to the near-IR ($\sim$770 nm), with a peak in the blue region ($\sim$412 nm) [2]. Until recently, the importance of NO$_2$ absorption has been largely ignored in the retrieval of oceanic parameters from satellite measurements. For example, in the retrieval of water-leaving radiances (Lws) from sea-viewing wide field-of-view sensor (SeaWiFS) and moderate-resolution imaging spectroradiometer (MODIS) measurements, the effect of NO$_2$ absorption is not considered at all. The results from the Global Ozone Measuring Experiment (GOME), Scanning Imaging Absorption Spectrometer for Atmospheric Cartography (SCIAMACHY), and, most recently, from the Ozone Measuring Instrument (OMI) sensors clearly

show the presence of NO_2 near the Eastern Coast of the United States and Northern Europe. Over the Eastern United States, the NO_2 column amount often exceeds 1 Dobson Unit [(DU), $\sim 2.69 \times 10^{16}$ molecules/cm²]. Although high concentrations of NO_2 are typically confined to industrial areas and have relatively short lifetimes in the boundary layer (for example, the NO_2 lifetime is of the order of 27 h [3], recent studies have shown that NO_2-rich pollution hot spots can spread over long distances for several days [4–7]. NO_2 also shows a seasonal cycle with a maximum in the winter months. Boundary layer NO_2 has a strong diurnal variation with a maximum at approximately 10 a.m. in the morning and a gradual decrease throughout the afternoon, and there can be significant daily variation in this pattern depending on the daily meteorology and on the strength of the sources [8].

In this paper, we report the results of a sensitivity study that examines how top-of-atmosphere (TOA) reflectances in the visible change with variations in the NO_2 amount in the troposphere, and provide details of an NO_2 correction algorithm that enables accurate retrieval of Lws in the presence of varying amount of NO_2 concentration over the ocean. Our radiative transfer sensitivity calculations show that, under high NO_2 conditions ($\sim 1 \times 10^{16}$ molecules/cm²), the error in TOA reflectance in the blue channels of the SeaWiFS and MODIS instruments is approximately 1%. This translates into an approximately 10% error in Lw for clear waters. As these Lws decrease with an increase in chlorophyll, colored dissolved organic matter (CDOM), and nonalgal suspended particles near the coast, the relative error in the Lws increases. We have applied the NO_2 atmospheric correction algorithm to 52 MODIS scenes off the Eastern Coast of the United States with large amounts of NO_2 in the atmosphere, and results from one such scene on 15 April 2005 are presented and discussed in this paper.

2. Radiative Transfer Simulations (Forward Modeling)

Following the radiative transfer (RT) theory, it is customary to write the TOA reflectance, ρ_t, over a rough ocean surface as

$$\rho_t(\lambda, \theta_o, \theta, \varphi, v) = \rho_{path}(\lambda, \theta_o, \theta, \varphi)$$
$$+ t_1 t_d \rho_g(\lambda, \theta_o, \theta, \varphi, v)$$
$$+ t_2 t_d \rho_{wc}(\lambda, \theta_o, \theta, \varphi, v)$$
$$+ t_3 t_d \rho_{wL}(\lambda, \theta_o, \theta, \varphi, v), \quad (1)$$

where, λ, θ_o, θ, φ, and v, refer to the wavelength, the solar zenith angle, the sensor view and azimuth angles, and the wind speed over the ocean surface, respectively. The definitions of the other terms are as follows: ρ_{path}, is the path reflectance to the sensor owing to multiple scattering in the atmosphere by air molecules (Rayleigh scattering) and aerosols (Mie scattering). ρ_g, ρ_{wc}, and ρ_{wL}, respectively, are the glint (ρ_g), white cap (ρ_{wc}), and water-leaving (ρ_{wL}) reflectances at the ocean surface, and t_1, t_2, t_3 are their respective transmittances in the direction (θ, φ)

through the atmosphere. $t_d = E_d/\mu_o F_o$, where E_d is the sum of the downwelling direct and diffuse irradiances on the ocean surface, F_o is the extraterrestrial solar irradiance at the top of the atmosphere, and μ_o is the cosine of the solar zenith angle, θ_o. Although the numerical values of the three transmittances (t_1, t_2, and t_3) are very close to one another, they are in fact different because of different illumination conditions at the base of the atmosphere. For example, in the case of white caps, the upwelling radiation at the base of the atmosphere is generally considered isotropic and unpolarized, whereas in the case of sunglint and Lws, the upwelling radiation is anisotropic and polarized.

In Eq. (1), we have defined reflectance as

$$\rho(\lambda, \theta_o, \theta, \varphi, v) = \pi L(\lambda, \theta_o, \theta, \varphi, v)/E(\lambda), \quad (2)$$

where, L and E, respectively, are the upwelling radiance and the downwelling irradiance. For path reflectance $E = \mu_o F_o$. For glint, whitecaps and water-leaving reflectance, $E = E_d$.

To simulate the TOA reflectances, we used a modified version of Ahmad–Fraser's code [9]. The code properly accounts for the Fresnel reflection from the rough ocean surface as well as all orders of scattering and polarization of the diffuse radiation in the atmosphere. It can simulate reflectance for any wavelength in the UV, visible, or near-IR part of the spectrum. For this study, we selected the visible bands of SeaWiFS and MODIS sensors. Table 1 shows the band-average values of Rayleigh scattering optical thickness, $\tau(\lambda)$, and NO_2 cross section, σ, for the visible and near-IR bands of the two instruments. The band-average optical thickness was computed using the following relation:

$$\langle \tau(\lambda) \rangle = \sum \tau(\lambda) F_o(\lambda) R(\lambda)/\sum F_o(\lambda) R(\lambda), \quad (3)$$

where R is the instrument response function. In Eq. (3) the values of $\tau(\lambda)$ were calculated at 1 nm intervals using a constant value of 0.0279 for the molecular anisotropy. The solar flux values were taken from Thuillier *et al.* [10] and the spectral response function values from Barns *et al.* [11,12]. For NO_2, we used Vandaele *et al.* [2] absorption cross section (square centimeters per molecule) and calculated a band-average value using an expression similar to the one given in Eq. (3). It should be noted here that the NO_2 cross-section values are for a temperature of 294 K. In our RT calculations, the values were corrected for the actual temperature of each calculation layer given by a mean climatological profile for midlatitude summer.

In our RT simulations, the aerosol size distribution is characterized by a bimodal lognormal distribution (C80), and these aerosols are distributed vertically according to Elterman's [13] distribution. The aerosols are very weakly absorbing with a single scattering albedo at 412 nm of 0.988. C80 is similar to

Table 1. Rayleigh Scattering Optical Thickness (τ) and NO$_2$ (σ) Absorption Cross Section (10^{-19} cm^2 per Molecule) for the SeaWiFS and the MODIS-Aqua Visible and Near-IR Bands[a]

SeaWiFS										
Band (nm)	412	443	490	510	555	670	765	865	—	—	—
τ (Rayleigh)	0.3136	0.2346	0.1546	0.1330	0.0947	0.04450	0.0256	0.0169	—	—	—
σ (NO$_2$)	5.915	4.913	2.667	1.995	0.874	0.085	0.080	0.000	—	—	—

MODIS										
Band (nm)	412	443	469	488	531	551	555	645	667	670	748
τ (Rayleigh)	0.3092	0.2363	0.1911	0.1590	0.1126	0.0990	0.0943	0.0508	0.0444	0.0415	0.0285
σ (NO$_2$)	7.724	4.916	3.897	2.802	1.437	1.124	0.877	0.070	0.080	0.090	0.10

[a]The table also includes four MODIS land-bands. Also, the values for bands longer than 555 nm are average values taken from the graph in Vandaele *et al.* [2].

coastal aerosol distributions that are used operationally for the atmospheric correction of the SeaWiFS and MODIS data [14]. It is constructed from Shettle and Fenn's [15] tropospheric and oceanic models for a relative humidity value of 80%.

We use five NO$_2$ profiles in the RT simulations. Three of these profiles are constructed by combining the mean stratospheric NO$_2$ profile obtained from the Goddard Chemical Transport Model (CTM) with three tropospheric NO$_2$ profiles obtained from the Global Earth Observing System CHEMistry (GEOS-CHEM) 3D model representing low, moderate, and high amounts of NO$_2$ pollution [16] (Fig. 1). Two additional tropospheric NO$_2$ profiles are created by averaging the low and moderate, and the moderate and high tropospheric NO$_2$ profiles. The amounts of NO$_2$ in the five profiles are 2.847×10^{15}, 3.069×10^{15}, 3.291×10^{15}, 7.301×10^{15}, and 1.132×10^{16} molecules/cm^2, respectively. These total column amounts are well below typical polluted-day values (~ 3 to 6×10^{16} molecules/cm^2, 1 to 2 DU) observed at Goddard Space Flight Center [8].

The lower boundary of our model atmosphere is a rough ocean surface where it is assumed that the slope probability distribution of the capillary waves follows the Cox and Munk [17] wind-direction inde-

Fig. 1. Three of the NO$_2$ profiles used in the RT simulations.

pendent distribution. This distribution is characterized by wind speed alone. A wind speed of 4 m/s is used in the simulations.

Finally, we carry out the simulations for a molecular atmosphere and molecular plus aerosol atmosphere in the absence of NO$_2$ gas, and then we repeat the simulations with all the NO$_2$ profiles described above. In these simulations, the contributions from Lws and white caps are not considered.

3. Results

Although RT simulations are performed for all bands of SeaWiFS and MODIS listed in Table 1, we report here only the results for the 412 nm band. This band has the largest value of NO$_2$ absorption cross section and largest value of the Rayleigh optical thickness, and therefore shows the largest change in the TOA reflectance. Also, Lw values at 412 nm are relatively low (~ 0.1 mW/cm^2/μm/sr) in coastal waters where absorption by CDOM and nonalgal particles is high. Retrieved negative values of Lw(412) are frequently observed, implying some additional absorption in the atmosphere that is not included in the standard retrieval algorithm. Other bands, to a lesser degree, show similar results. Figure 2(a) shows the TOA reflectance for the molecular and molecular plus aerosol models of atmosphere. For both models of the atmosphere, the reflectance increases with an increase in the view and the solar zenith angles. In addition, the TOA reflectance increases with aerosols in the atmosphere, however, only by $\sim 10\%$. Also, the increase is very weakly dependent on the view angle. The increase in the reflectance with view and solar zenith angles can be understood by realizing that the increase in the values of these two angles increases the slant path, and hence the scattering centers, in the atmosphere. Similarly, the addition of aerosols further increases the scattering centers. However, aerosols have smaller values of the phase function in the backward directions, which makes them less efficient than air molecules. Figure 2(b) shows the effect of NO$_2$ absorption on the TOA reflectance, where the ordinate is the ratio of reflectance with and without NO$_2$ in the model atmosphere. As expected, the TOA reflectance ratio decreases with an increase in NO$_2$ amount, and the rate of decrease is larger for
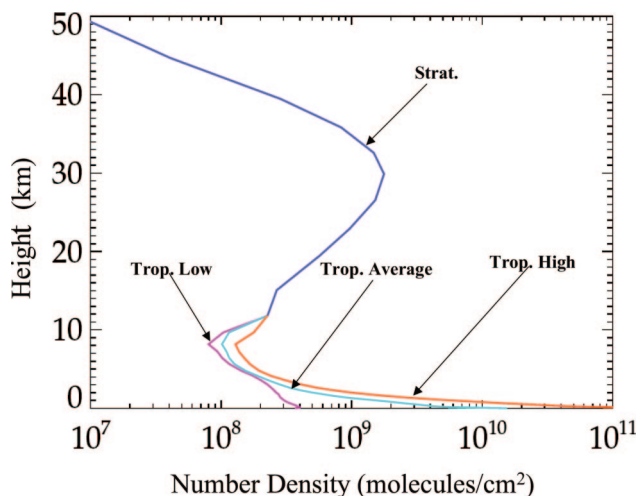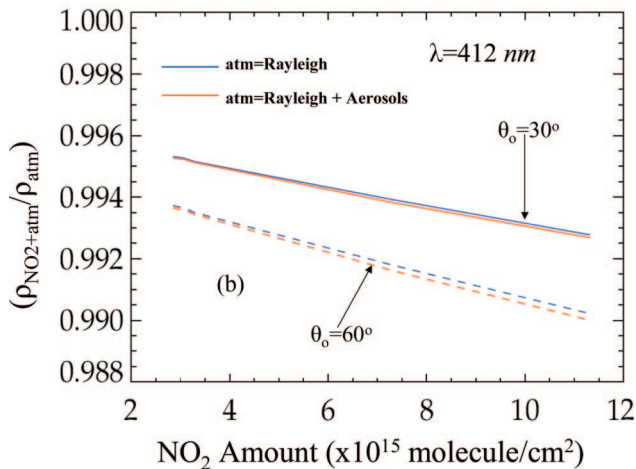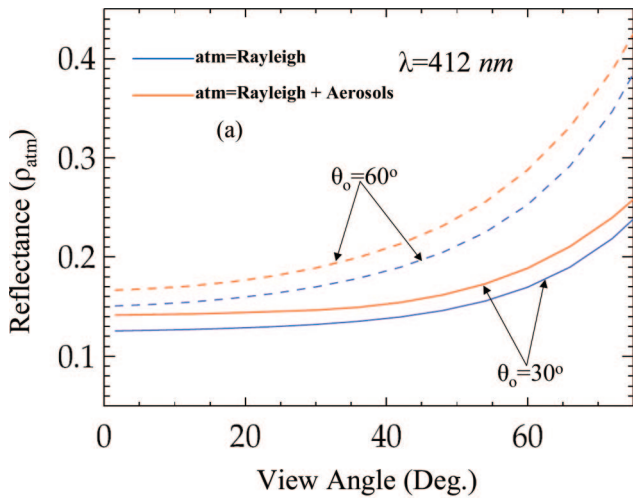
Fig. 2. (a) Top-of-atmosphere (TOA) reflectances for molecular and molecular plus aerosol models of atmosphere with a rough ocean surface at the lower boundary. An aerosol optical thickness of 0.2 is used in the simulations. Simulations for $\theta_o = 30°$ are represented by solid curves and for $\theta_o = 60°$ by dashed curves. (b) Ratio of TOA reflectances in the nadir direction with and without NO_2 in the models of atmosphere as a function of NO_2 amount. Other details are the same as in (a).

$\theta_o = 60°$ than for $\theta_o = 30°$. This is because of larger slant path for $\theta_o = 60°$, which results in more scattering and hence more absorption. We also note that the relative decrease in the TOA reflectance ratio is practically independent of the aerosol amount in the atmosphere. This suggests that an atmospheric correction algorithm can be developed that does not require *a priori* knowledge of aerosols properties in the atmosphere.

The azimuth dependence of the relative change in the TOA reflectance with and without NO_2 in the atmosphere is shown in Fig. 3. The results are for a highly NO_2 polluted (1.13×10^{16} molecules/cm^2) molecular atmosphere. We find that the relative change in the TOA reflectance even at large solar zenith angles (for example, $\theta_o = 60°$) is almost independent of the azimuth angle. We also find similar results when a small amount of aerosols ($\tau < 0.2$) is added to
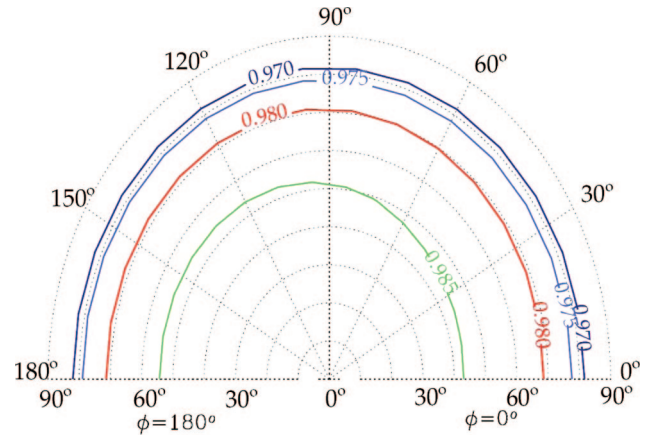

Fig. 3. Ratio of TOA reflectances with and without NO_2 for a molecular atmosphere for $\theta_o = 60°$.

the atmosphere. In Section 4, we use these results in developing an atmospheric-correction algorithm for water-leaving reflectances (ρ_w) in the presence of NO_2.

4. NO_2 Correction Algorithm

A. Path Reflectance Correction

For most absorbing gases that reside in the stratosphere or upper troposphere, a simple Beer's law correction is sufficient to remove the effect of absorption from the reflectance measured at TOA. The Beer's law correction can be written as

$$\rho_{corr} = \rho_{obs} \exp[\alpha N(\sec \theta_o + \sec \theta)], \quad (4)$$

where α and N are the absorption cross section and column amount of the absorbing gas, respectively; ρ_{obs} and ρ_{corr} are the TOA reflectance with and without the absorbing gas, respectively; and ($\sec \theta_o + \sec \theta$) is the geometric air mass factor (AMF). For an absorbing gas that resides in the lower troposphere, an atmospheric-correction algorithm solely based on geometric AMF is not sufficient. This is because the absorption increases with multiple scattering by air molecules and aerosols in the atmosphere. For stratospheric absorbing gases, the use of the geometric AMF is valid because the effect of additional absorption due to scattering by air molecules is very small and in most cases can be ignored.

In the presence of tropospheric absorbing gases, it is important that we determine the AMF through the radiative transfer simulation. For this purpose, we rewrite Eq. (4) as

$$AMF = \ln(\rho_{corr}/\rho_{obs})/\alpha N. \quad (5)$$

To compute the AMF for the NO_2 gas, we used RT simulations for a standard molecular atmosphere with the five NO_2 profiles described earlier in this paper. Based on the results presented in Section 3,

Table 2. Polynomial Coefficients for the RT Derived AMF Using Average NO_2 Distribution[a]

	b_0	b_1	b_2	b_3	b_4	b_5
a_0	2.0686	−3.4509	3.4692	−1.3379	2.4680×10^{-1}	-1.7485×10^{-2}
a_1	−1.6280	5.4493	−4.3369	1.6747	-3.1165×10^{-1}	2.2266×10^{-2}
a_3	8.6136×10^{-1}	−1.8646	1.4819	-5.7382×10^{-1}	1.0712×10^{-1}	-7.6739×10^{-3}
a_4	-9.6001×10^{-2}	2.0243×10^{-1}	-1.6106×10^{-1}	6.2491×10^{-2}	-1.1692×10^{-2}	8.3924×10^{-4}

[a]The average NO_2 distribution is 3.291×10^{15} molecules/cm². The AMF is expressed as $AMF = \sum_0^3 a_i(\sec \theta_o)\sec^i \theta$ where $a_i(\sec \theta_o) = \sum_0^5 b_{ij} \sec^j \theta_o$.

the AMF determined for molecular atmosphere is equally applicable for molecular atmosphere with small amounts of aerosols ($\tau < 0.2$). It should be noted that the radiative transfer derived AMF depends on the Sun-view-angle geometry and the vertical profile of the NO_2 in the atmosphere. Also, based on the results presented in Fig. 3, we can ignore the azimuth dependence of AMF. In other words, the AMF determined for molecular atmosphere for one value of azimuth angle (for example, $\varphi = 96°$) should be equally applicable for all azimuth angles of SeaWiFS and MODIS observations, which are generally larger than 90°. Of course, the RT-derived AMF will continue to be dependent on the view and solar zenith angles and the NO_2 vertical profile in the atmosphere.

For operational processing of the data, it is more desirable (faster) to use an equation to compute a quantity than to use lookup tables to determine the value of the quantity. With this in mind, we parameterized the RT-derived AMF for $\varphi = 96°$ using polynomials in $\sec \theta$ and $\sec \theta_o$. We expressed the view angle dependence by a third-order polynomial in $\sec \theta$, and then each coefficient by a fifth-order polynomial in $\sec \theta_o$. That is

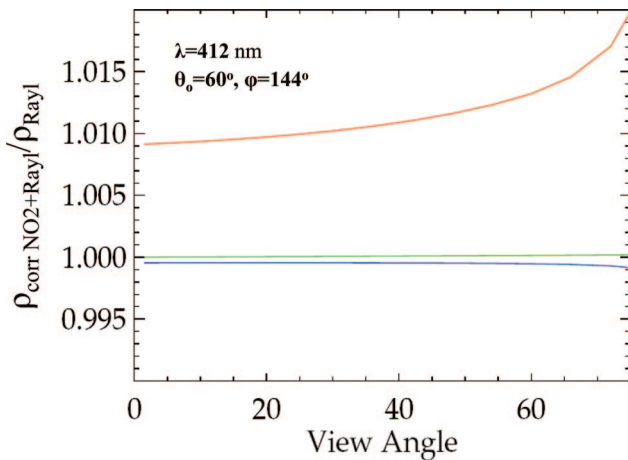$$AMF = \sum_0^3 a_i(\sec \theta_o)\sec^i \theta, \quad (6a)$$

where

$$a_i(\sec \theta_o) = \sum_0^5 b_{ij} \sec^j \theta_o. \quad (6b)$$

The coefficients of the polynomial fit are given in Table 2.

To test the RT-derived AMF correction algorithm, we used the polynomial coefficients derived for the average tropospheric NO_2 and $\varphi = 96°$ and computed the ratio of reflectances with and without NO_2 in the atmosphere. The results for low, average, and high tropospheric NO_2 are shown in Fig. 4. These results suggest that the AMF derived from the average tropospheric NO_2 profile will properly correct the TOA reflectances when the NO_2 amount in the troposphere is less than that in the average tropospheric NO_2 profile, but it will overestimate the atmospheric correction when the NO_2 amount in the troposphere is higher than for the average NO_2 tropospheric profile. One reason for this overestimation is the fact that most of the NO_2, for large tropospheric column NO_2 amounts, is located very close to the low reflectivity boundary surface (rough ocean with reflectivity of a few percent), where there are proportionately very few photons that contribute to the TOA reflectances. This can be seen from the graph in Fig. 5 where the sensitivity, $\Delta\rho_{top}/\Delta NO_2$, of a layer is plotted against height. The sensitivity is often called the weighting function, and it shows change in the TOA reflectance when the NO_2 amount in a layer is perturbed by a
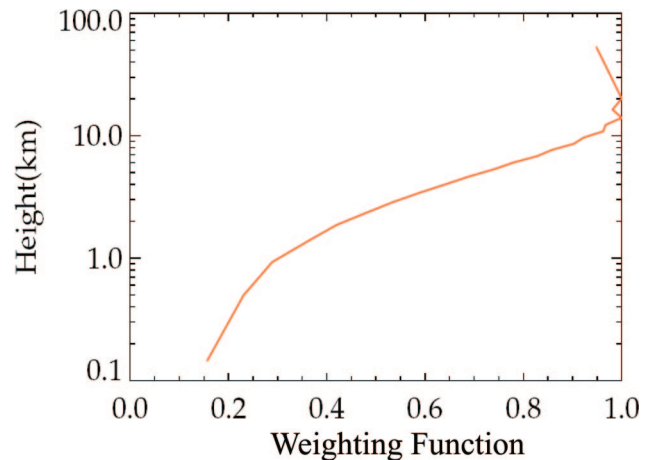

Fig. 4. Results of atmospheric correction using RT-based AMF computed for a molecular atmosphere with low (blue curve, 2.847×10^{15} molecules/cm²), average (green curve, 3.291×10^{15} molecules/cm²), and high (brown curve, 1.132×10^{16} molecules/cm²) amount of NO_2. The AMF was computed for $\varphi = 96°$.

Fig. 5. NO_2 weighting function, ($\Delta\rho_{top}/\Delta NO_2$), for high amount of NO_2 (1.132×10^{16} molecules/cm²) in the atmosphere. The results are for $\theta_o = 30°$.
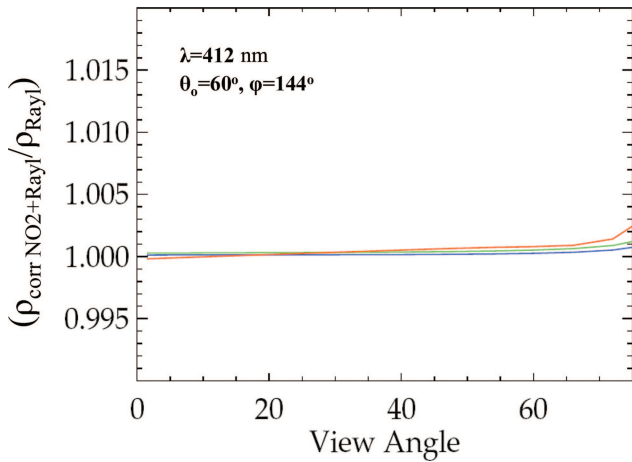
Fig. 6. Atmospheric correction with the RT-based AMF after correcting for NO_2 amount from 200 m to the surface. Other details are the same as in Fig. 4.

Fig. 7. Atmospheric correction with geometric AMF after correcting for NO_2 amount from 200 m to the surface. Other details are the same as in Fig. 4.

small amount. The graph is normalized to unity at its maximum value. This graph clearly shows that TOA reflectance is less sensitive to increases in NO_2 near the bottom boundary of the atmosphere. The same is not true for ρ_w.

To compute ρ_{corr} from Eq. (4) the weighting function results suggest that we can ignore the NO_2 amount near surface because the backscattered reflectance, ρ_{obs}, is not sensitive to NO_2 amounts near surface. Therefore, we decided not to include the amount of NO_2 from 200 m to the surface in the calculation of ρ_{corr} from Eq. (4). The value of 200 m was selected because it was close to the altitude of the top level of the bottom-most layer in the RT calculations.

We applied this new algorithm to the three (low, average, and high) tropospheric NO_2 profiles shown in Fig. 1 and found that the algorithm works extremely well (Fig. 6). The maximum error in all cases was of the order of 0.15%. This shows that the correction is practically independent of the view angle. We find similar results for all solar zenith angles, θ_o, less than 72°.

The idea that we can ignore the NO_2 amount from 200 m to the surface prompted us to ask whether we can use the corrected NO_2 amount with geometric AMF to accurately determine the TOA reflectance in the presence of high NO_2 amounts in the atmosphere. We tested this hypothesis on model atmospheres with the three, low, average, and high tropospheric NO_2 amounts and found that this method also produced results that are almost as good as with the AMF derived with the help of radiative transfer calculations. The results for $\theta_o = 60°$ are shown in Fig. 7. At larger solar zenith angle (for example, $\theta_o = 72°$), we found a weak view-angle dependence in the atmospheric correction.

B. Water-Leaving Reflectance Correction

In the preceding sections, we have described the NO_2 correction only for the path reflectance that results from the scattering of solar irradiance by aerosols
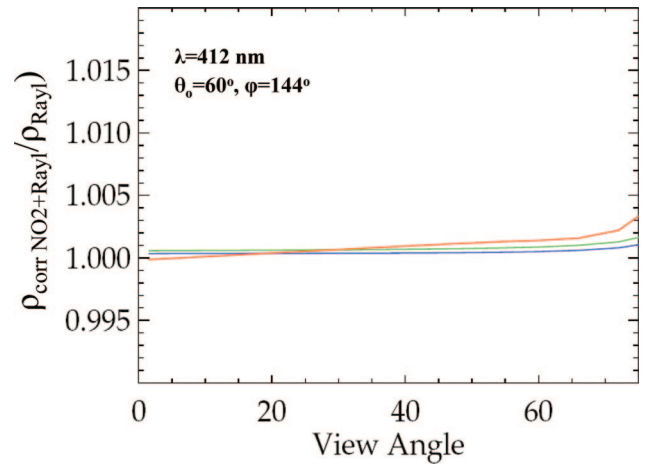
and air molecules. Now we will describe the NO_2 correction for the Lw from the ocean. Note that in the absence of sun-glint and whitecaps, the observed reflectance at the TOA is the sum of path reflectance and the water-leaving reflectance corrected for atmospheric transmittance. That is

$$\rho_t(\lambda, \theta_o, \theta, \varphi, v) = \rho_{path}(\lambda, \theta_o, \theta, \varphi) + t_3 t_d \rho_{wL}(\lambda, \theta_o, \theta, \varphi, v). \quad (7)$$

To correct the path reflectance, we multiply both sides of Eq. (7) by $\exp[\alpha N(\sec \theta_o + \sec \theta)]$ and we get

$$\rho_t \exp[\alpha N'(\sec \theta_o + \sec \theta)] = \rho_{path} \exp[\alpha N'(\sec \theta_o + \sec \theta)] + [t_3 \exp(\alpha N' \sec \theta)] \times [t_d \rho_{wL} \exp(\alpha N' \sec \theta_o)]. \quad (8)$$

Here N' is the amount of NO_2 from 200 m to the TOA, where, for clarity purposes, we have dropped the arguments of ρ_t, ρ_{path}, and ρ_{wL}. Based on RT simulations, we find that, in the above equation, the path reflectance is correct to within ±0.2%, and the error in the transmission term: $[t_3 \exp(\alpha N' \sec \theta)]$ also is approximately ±0.2%. However, the water-leaving reflectance term: $[t_d \rho_{wL} \exp(\alpha N' \sec \theta_o)]$ does not have the same accuracy. Simulation studies show that under a high column NO_2 senario, the error in the water-leaving reflectance term: $[t_d \rho_{wL} \exp(\alpha N' \sec \theta_o)]$ can vary from 0.5% near the nadir direction to ~1.5% at approximately a 70° view angle. The reason for this error is that the water-leaving reflectance, ρ_{wL}, depends on the total downwelling irradiance on the ocean surface, which, in turn, depends on the total amount of NO_2 molecules (N) and not the corrected amount (N') that appears in the atmospheric path radiance correction. Simulation results also show that the error in the water-leaving reflectance term reduces to approximately 0.2% when N' is replaced with N.

The results described above suggest that if the observations are made only in one wavelength band, then it is not possible to seperate the atmospheric path reflectance from the water-leaving reflectance, and the correction for the path reflectance will always leave some error in the water-leaving reflectance. However, with SeaWiFS and MODIS sensors, where the atmospheric correction is determined from the near-IR or shortwave IR (SWIR) channels, we can further reduce the error in the water-leaving reflectance. This is done in the following empirical way. We propose that for NO_2 absorbing wavelength bands (for example, centered at 412 and 443 nm common to both instruments), we determine the atmospheric correction from the near-IR or SWIR channels as it is routinely done in the operational processing of SeaWiFS and MODIS data. However, instead of subtracting the atmospheric correction terms from the corrected TOA reflectance, we reduce the atmospheric correction terms (including the Rayleigh reflectance) for the NO_2 absorption in the atmosphere. This can be done by multiplying the computed path reflectance by $\exp[-\alpha N'(\sec \theta_o + \sec \theta)]$. Next, we subtract the computed path reflectance for NO_2 from the observed TOA reflectance, which gives us, $\Delta\rho_{obs} = t_3 t_d \rho_{wL}$, the TOA value for the water-leaving reflectance in the presence of NO_2 in the atmosphere. To get the NO_2 corrected value of water-leaving reflectance, all we have to do is multiply $\Delta\rho_{obs}$ by $\exp(\alpha N' \sec \theta)\exp(\alpha N \sec \theta_o)$. That is

$$\exp(\alpha N' \sec \theta)\exp(\alpha N \sec \theta_o)\Delta\rho_{obs}$$
$$= t_3 \exp(\alpha N' \sec \theta)t_d \rho_{wL} \exp(\alpha N \sec \theta_o). \quad (9)$$

Note that $t_3 = t_3 \exp(\alpha N' \sec \theta)$ is the transmission term, and $\rho'_{wL} = t_d \rho_{wL} \exp(\alpha N \sec \theta_o)$ is the water-leaving reflectance term, both in the absence of NO_2 in the atmosphere. To get the corrected water-leaving reflectance, we rewrite Eq. (9) as

$$\rho'_{wL} = \exp(\alpha N' \sec \theta)\exp(\alpha N \sec \theta_o)\Delta\rho_{obs}/t'_3, \quad (10)$$

where t'_3 values can be obtained from the lookup tables used for SeaWiFS and MODIS operational data reduction.

5. Case Study

We have tested our new NO_2 atmospheric correction algorithm on a number of MODIS scenes off the Eastern Coast of the United States and found that the correction significantly increases the estimated water-leaving radiance in the 412 nm band of the instrument. We processed the data using both the RT-derived AMF and the geometric AMF and found very similar results. The results from one case study using the geometric AMF are described below.

We selected MODIS-Aqua data from 11 April 2005 over the Northeastern Coast of the United States. Figure 8(a) shows the red–green–blue (RGB) image, which was produced by combining the radiances from

469, 555, and 645 nm bands of the MODIS instrument. The scene is generally clear, except that there is an aerosol layer over the ocean that appears to be coming from the New Jersey area. Figure 8(b) shows the retrieved aerosol optical thickness (AOT) over the same scene in the 869 nm band. We find that the AOT is ~0.2 in the plume, but it is generally less than 0.1 over most of the scene and over some parts of the ocean the AOT is ~0.04.

The tropospheric NO_2 amounts, shown in Figure 8(c), were obtained from the ozone measuring instrument (OMI) onboard Aura, which was launched on 15 July 2004 and flies in formation with MODIS-Aqua. The OMI NO_2 data were processed at the Goddard Space Flight Center (GSFC) and provided by the NO_2 Processing Team. The NO_2 data used in our atmospheric correction algorithm consisted of daily total NO_2 and tropospheric NO_2 amounts given at every $0.25° \times 0.25°$ grid. Presently, data from 29 September 2004 to 14 May 2006 are available; however, the current products are provisional in nature and may be 50% too low as determined from ground-based measurements [8].

In the OMI NO_2 image, we find NO_2 amounts greater than 2×10^{16} molecules/cm^2 over New York City and the surrounding oceanic area. We also find very significant concentrations ($\sim 1 \times 10^{16}$ moelcules/cm^2) over a much larger area of the ocean that extends from Delaware–New Jersey in the south to New York Long Island in the north. In addition, over most of the cloud-free ocean area, the NO_2 amounts are $\sim 5 \times 10^{15}$ molecules/cm^2. Figure 8(d) shows the nLw in the 412 nm band from the current operational processing of MODIS. Comparing Fig. 8(c) with 8(d) we find that in the region where tropospheric NO_2 amount is very high ($>1.6 \times 10^{16}$ molecules/cm^2), the retrieved nLw is very low (<0.1 mW/cm^2/μm/sr). The incorporation of the NO_2 atmospheric correction [Fig. 8(e)] results in higher nLw values over high NO_2 concentration areas [Fig. 8(c)]. Also, the region with a very small value of nLw (<0.1 mW/cm^2/μm/sr) in Fig. 8(d) has practically disappeared.

To get a general sense of the shift in nLw for the 412 nm band radiance, we show, in Fig. 9, a histogram of nLw radiances with and without NO_2 correction. For this scene, the peak of the distribution in the current operational retrieval is 0.354 mW/cm^2/μm/sr, and with the NO_2 correction the peak shifts to 0.428 mW/cm^2/μm/sr. This suggests that in the coastal areas under high NO_2 amount the current operational processing underestimates the nLw in the blue channels of the SeaWiFS and MODIS sensors. In this particular case, the underestimation is $\sim 19\%$, based on the shift of the mode. The underestimation in the mean value of nLw for the scene is $\sim 17\%$. This is significant because for the MODIS sensor the measurement error in nLw due to the digitization error in the TOA reflectances over case 2 waters is $\sim 2.5\%$.
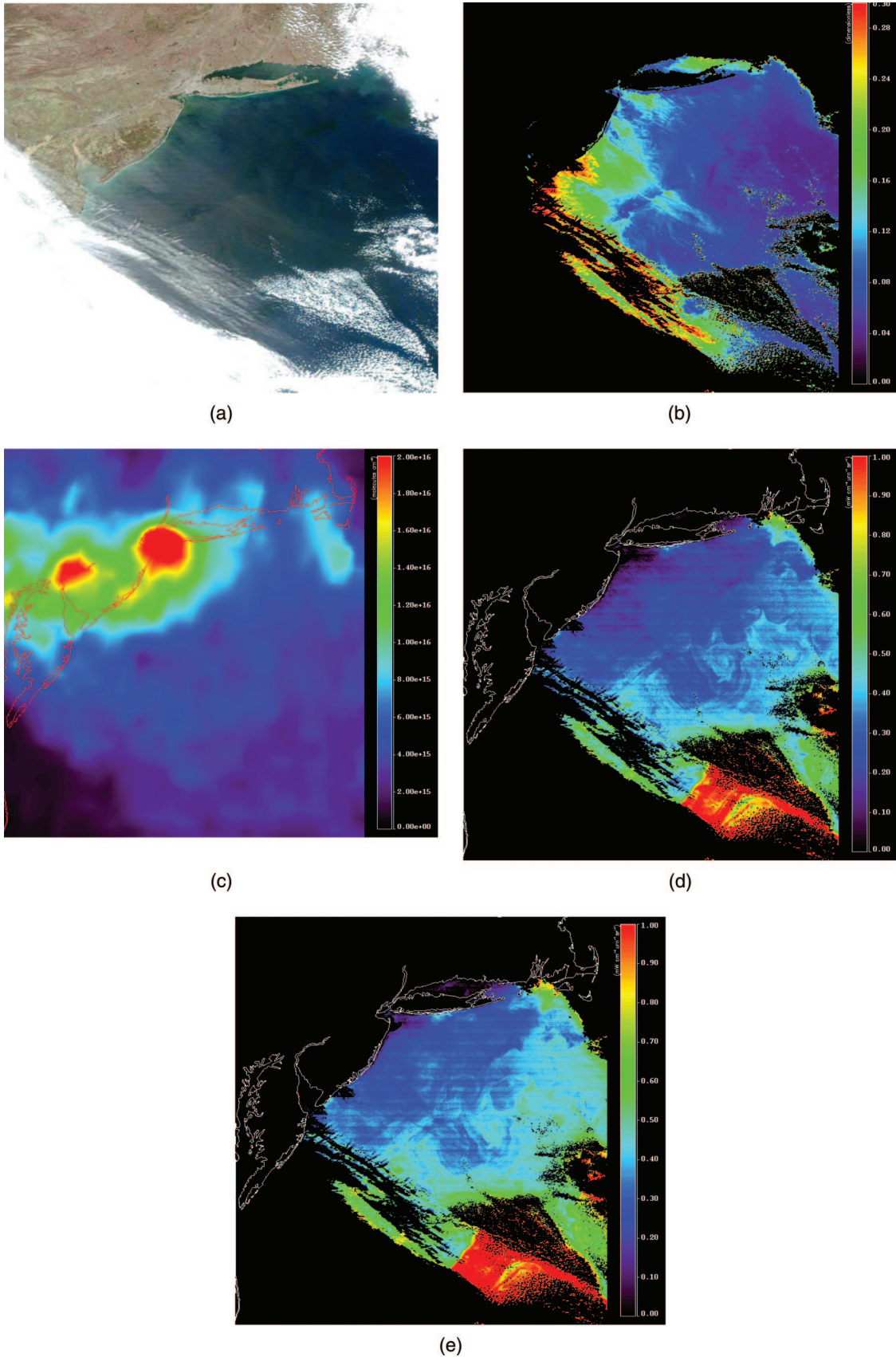
Fig. 8. (a) RGB image of a MODIS-Aqua scene from 11 April 2005 over the Northeastern coast of the United States. (b) MODIS aerosol optical thickness of 869 nm over the Northeastern coast of the United States on 11 April 2005. (c) OMI tropospheric NO_2 amount over the Northeastern coast of the United States on 11 April 2005. (d) nLw band of 412 nm, from the current operational algorithm for the MODIS scene shown in (a). (e) NLw band of 412 nm using the NO_2 correction algorithm for the MODIS scene shown in (a).
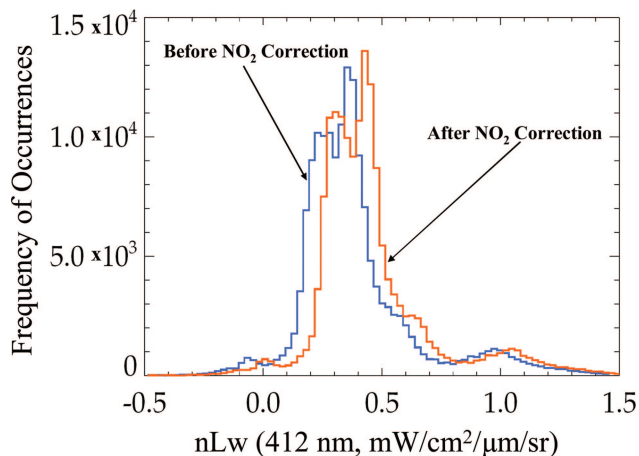
Fig. 9. Histogram of the 412 nm band nLw with (blue curve) and without NO_2 (orange curve) correction for the MODIS scene shown in Fig. 8(a).

6. Conclusions

We have presented the details of an atmospheric-correction algorithm that allows accurate retrieval of water-leaving radiances in the presence of varying amounts of NO_2 in the atmosphere over ocean. The correction algorithm is based on Beer's law and it utilizes the OMI-derived NO_2 values, which are corrected for the boundary layer NO_2 (200 m to the ground). The boundary layer correction is obtained from a simple empirical relation that is derived from the tropospheric NO_2 profiles obtained from the GEOS-CHEM 3D model. Our analyses show that with the boundary layer correction the Beer's law with geometric AMF gives results as good as those obtained from the RT-based AMF. Finally, over the Chesapeake Bay area, our NO_2 correction algorithm reduces the frequency of negative normalized water-leaving radiance (nLw) estimates in the 412 nm band of MODIS data and increases the nLw values in the same band. For the case study scene presented in this paper, the increase in the mean value of nLw for the 412 nm band is ~17%. This is significant because for the MODIS sensor the measurement error in nLw due to the digitization error in the TOA reflectances over case 2 waters is ~2.5%.

References

1. S. Solomon, R. W. Portmann, R. W. Saders, J. S. Daniel, D. W. Madsen, B. Bartram, and E. G. Dutton, "On the role of nitrogen dioxide in the absorption of the solar radiation," J. Geophys. Res. **99,** 12047–12058 (1999).
2. A. C. Vandaele, C. Hermans, P. C. Simon, M. Carleer, R. Colin, S. Folly, M. F. Merienne, A. Jenouvrier, and B. Coquart, "Measurements of the NO_2 absorption cross section from 42000 cm-1 to 10000 cm-1 (238-1000 nm) at 220 K and 294 K," J. Quant. Spectrosc. Radiat. Transfer **59,** 171–184 (1998).
3. C. Leue, M. Wenig, T. Wagner, O. Klimm, U. Platt, and B. Jahne, "Quantitative analysis of NOx emissions from Global Ozone Monitoring Experiment satellite image sequences," J. Geophys. Res. **106,** 5493–5505 (2001).
4. L. Jaegle, D. J. Jacob, Y. Wang, A. J. Weinheimer, B. A. Ridley, T. L. Campos, G. W. Sachse, and D. E. Hagen, "Sources and chemistry of NOx in the upper troposphere over the United States," Geophys. Res. Lett. **25,** 1705–1708 (1998).
5. A. Stohl, H. Huntrieser, A. Richter, S. Beirle, O. R. Cooper, S. Eckhardt, C. Forster, P. James, N. Spichtinger, M. Wenig, T. Wagner, J. P. Burrows, and U. Platt, "Rapid intercontinental air pollution transport associated with a meteorological bomb," Atmos. Chem. Phys. **3,** 969–985 (2003).
6. D. Schaub, A. K. Weiss, J. W. Kaiser, A. Petritoli, A. Richter, B. Buchmann, and J. P. Burrows, "A transboundary transport episode of nitrogen dioxide as observed from GOME and its impact in the Alpine region," Atmos. Chem. Phys. **5,** 23–37 (2005).
7. N. Spichtinger, M. Wenig, P. James, T. Wagner, U. Platt, and A. Stohl, "Satellite detection of a continental-scale plume of nitrogen oxides from boreal forest fires," Geophys. Res. Lett. **28,** 4579–4582 (2001).
8. A. Cede, J. Herman, A. Richter, N. Krotkov, and J. Burrows, "Measurements of nitrogen dioxide total column amounts at Goddard space flight center using a brewer spectrometer in direct sun mode," J. Geophys. Res. **111,** D05304 (2006).
9. Z. Ahmad and R. S. Fraser, "An iterative radiative transfer code for ocean-atmosphere systems," J. Atmos. Sci. **39,** 656–665 (1982).
10. G. Thuillier, M. Herse, P. C. Simon, D. Labs, H. Mandel, D. Gillotay, and T. Foujols, "The solar spectral irradiance from 200 to 2400 nm as measured by the SOLSPEC spectrometer from the ATLAS 1-2-3 and EURECA missions," Sol. Phys. **214,** 1–22 (2003).
11. R. A. Barnes, W. L. Barnes, W. E. Esaias, and C. McClain, "Prelaunch acceptance report for the SeaWiFS radiometer," NASA Technical Memorandum 104566, Vol. 22 (1994).
12. R. A. Barnes, A. W. Holmes, W. L. Barnes, W. E. Esaias, C. McClain, and T. Svitek, "SeaWiFS prelaunch radiometric calibration and spectral characterization," NASA Technical Memorandum 104566, Vol. 23 (1994).
13. H. R. Gordon, "Atmospheric correction of ocean color imagery in the Earth Observing System era," J. Geophys. Res. **102,** 17081–17106 (1997).
14. J. Elterman, "Parameters for attenuation in the atmospheric windows for fifteen wavelengths," Appl. Opt. **3,** 745–749 (1964).
15. E. P. Shettle and R. W. Fenn, "Models for the aerosols of the lower atmosphere and the effect of the humidity variation on their optical properties," Rep. AFGL-TR-79-0214 (U.S. Air Force Geophysical Laboratory, Hanscomb Air Force Base, Mass., 1997).
16. E. J. Bucsela, E. A. Celarier, M. O. Wenig, J. F. Gleason, J. P. Veefkind, K. F. Boersma, and E. J. Brinksma, "Algorithm for NO_2 vertical column retrieval from ozone monitoring instrument," IEEE Trans. Geosci. Remote Sens. **44,** 1245–1258 (2006).
17. C. Cox and W. H. Munk, "The measurement of roughness of the sea surface from photographs of the sun glitter," J. Opt. Soc. Am. **44,** 838–850 (1954).